ASTFE American Society of Thermal and Fluids Engineers

Proceedings of the 2nd Thermal and Fluids Engineering Conference
April 2-5, 2017, Las SAND2016-10465C

TFESC-17710

Modeling Aerodynamic Break-up of Liquid Drops in a Gas Flow with Molecular Dynamics Analogy Methods

Alexander L. Brown* **and Flint Pierce**

Sandia National Laboratories, PO Box 5800, Albuquerque, NM, 87185-1136, USA

ABSTRACT

The break-up of liquid drops is an important phenomenology for many applications. We approach this problem with the objective to improve methods for handling the modeling of the impulse and impact dispersal of liquids in transportation accident scenarios. These scenarios can be distinguished from many other simpler problems due to the quantity of liquid and the complexity of the intermediate liquid morphology. These differences necessitate alternative approaches to the problem. We have recently implemented a model for inter-particle forces between particles in a Lagrangian/Eulerian CFD code. The inter-particle force model is inspired by molecular dynamics methods, and employ a Lennard-Jones attractive force and a spring-based repulsive force. The Lennard-Jones parameters are related to the bulk fluid properties through a theoretical relationship model. Methods are necessary for modifying the single particle aerodynamic drag term depending on the new notion of particle connectivity. We want to evaluate these methods for potential utilization in practical simulations. Classical break-up tests for drops in flows suggest a critical Weber number relating to the onset of break-up for a drop. We seek to replicate these data with our model methods as a preliminary step before deploying the method in larger-scale practical environments.

KEY WORDS: Multiphase fluid, drop break-up

NOMENCLATURE

Symbol	*Unit*	*Description*	*Greek*	*Unit*	*Description*
C	-	Fit Constant	γ	M/T^2	Surface Tension
C_D	-	Drag Coefficient	ε	ML/T^2	Lennard-Jones Potential Energy
d	L	Diameter	ρ	M/L^3	Density
f_S	-	Drag limiter scaling factor	σ	L	Lennard-Jones Distance
K	-	f_{S1} Exponent constant	ω	1/T	Spring angular frequency
k	M/T^2	Spring Constant			
$\vec{k}$	-	Connectivity vector			
L	-	f_{S2} Exponent Constant	***Subscript***		***Description***
m	M	Mass			
N	-	Coordination Number			
$Proj$	-	Unit projection	LJ		Lennard-Jones
r	L	radius or separation distance	m		modified
T	-	Spring Period	o		Original or free-stream
Δt	T	Time step			
U	ML/T^2	Potential			
u	L/T	Velocity			
We	-	Weber number			

*Corresponding Author: albrown@sandia.gov

1. INTRODUCTION

The aerodynamic break-up of liquids in multi-phase fluid systems has long been a topic of research. This behavior fits in the broader category of multi-phase fluid flow. Some multi-phase capabilities are mature and reasonably well characterized, like low Reynolds number Newtonian Viscous flow. Yet, other capabilities such as the ability to predict a spray pattern emerging from a nozzle or to model break-up of high Weber number liquid drops are not mature in existing historical work.

The dispersal of contained liquids from an inertial or impulse induced spread has been the topic of model development at Sandia for the past several years (e.g., Brown et al., 2012, Brown and Pierce, 2015). This unique work has leveraged structural mechanics predictions (from the SIERRA/Presto code) to initialize the fluid field (in the SIERRA/Fuego code), and employs a Lagrangian/Eulerian coupled capability with a dilute spray assumption to model the subsequent fluid transport. This capability enables predictions otherwise unattainable using other methods for the dispersal of contained liquids due to high-speed impacts or impulses. Evaluation of several scenario predictions suggests that there may be some missing physics in the code coupling methodology that relates to the continuum nature of the liquid spray. The liquid continuum behavior is not presently captured by the Lagrangian dilute spray assumption employed for the liquid material in the CFD code. Past work has highlighted the potential necessity for improved models in this regard (see Brown and Pierce, 2015). Neighboring liquid drops have no notion of each other's existence, and this might be a significant omission for adjoining (and potentially physically connected) drops due to the neglected forces relating to the surface tension of the liquid. A model that can predict this behavior needs to exhibit an appropriate trade-off between efficiency and accuracy. With billions of drops often generated, it is not tractable to work with a model that resolves the interface of every drop. Nor can a volume or surface domain mesh be required to conform to the curvature of the liquid surface.

A method for aerodynamic drop break-up that has been widely implemented is known as the Taylor Analogy Break-up model, or TAB. The TAB model approximates a drop as a damped oscillator system, and tracks a deformation parameter. When the deformation parameter is sufficiently large, break-up is assumed. This model originated with the work of O'Rourke and Amsden (1987), and has been expanded upon in subsequent studies. Our particular implementation of this model is described in Brown et al. (2014). The TAB model is used with the Lagrangian/Eulerian coupled methods, but lacks the notion of a neighboring particle connectivity.

Others have addressed a similar problem from different perspectives. Oñate and Idelsohn have developed a method they term particle finite element method PFEM, which involves a gridless particle field and a contour reconstruction algorithm for surface forces. Notably, they have applied this method to simulations of breaking waves, among other applications (Idelsohn et al., 2004). Hermann and others have recently focused on the atomization of liquid from a jet in a cross-flow (Herrmann, 2013; Rana and Herrmann, 2011; Herrmann et al., 2011). A pinch-off from a continuum model is used to form incipient drops. Sprinkler spray atomization is similar in nature, but the recently described methods detailed by Wu et al. (2007) are not directly extensible to this application. Another continuum method is the nonlinear parabolic stability equations (PSE), first partially presented by Bertolotti et al. (1992) and later adapted for multi-phase problems. As reviewed by Cheung and Zaki (2011), this approach has evolved into a multiphase capability when coupled with interface capture (IC) schemes. In the case of Cheung and Zaki (2011), they use a Heaviside function with a disturbance equation at the interface. Another approach is the direct quadrature method of moments (DQMOM) method as described by Fox et al. (2008). It uses the Williams transport equation for Eulerian particle transport. The particle source and sink terms are managed through numerical approximations. While all viable approaches, none of these seems well suited for the present problem.

Of the above described methods, the TAB model and the PFEM method appear to be most closely aligned with our requirements. TAB lacks the ability to describe multi-particle system break-up. PFEM has the disadvantage of employing a surface reconstruction, which may be prohibitively expensive from a computational perspective.

Drop break-up behavior is well characterized in historical testing, which includes some of the more recent work of Hsiang and Faeth (1992), Theofanous et al., (2007), and Flock et al., (2012). The experimental work highlights the significance of the Weber number in the aerodynamic break-up of drops, and gives guidance on the structures and sizes obtained from the deforming and atomizing drops.

For this work we have employed the Sierra Low-Mach Module Fuego. Fuego is Sandia National Laboratories (SNL) CVFEM (Control Volume Finite Element Method) CFD code that has been used extensively to model scenarios as diverse as pool fires, building enclosure fires, propellant fires, composite fires, and impact and impulse driven liquid dispersion scenarios with drag induced particle breakup, as well as many others (Sierra, 2016). Fuego solves the incompressible Navier-Stokes equations in the fluid phase, and has the ability to couple the Eulerian fluid to a Lagrangian particle phase as well as a participating media radiation (PMR) model. Fuego also includes extensive turbulence and buoyancy models. The coupling between the Eulerian liquid and Lagrangian particle phases is two way so that the momentum, energy, and mass of the particle and fluid have corresponding source terms in both phases due to drag, heat and enthalpy, and mass exchange (particle/gas phase reactions), respectively. Previous to the current work, Lagrangian particles in Fuego were unable to interact with each other except indirectly through coupling to the fluid, and the particle phase was assumed to be at a low volume fraction. Because the coupling methods described earlier (Brown et al, 2012) suggest a need for improved modeling of particle interactions, we have extended the particle phase implementation by allowing force interactions between particles that lie near each other through a liquid-like force field (Lennard-Jones) in the flavor of a molecular dynamics simulation. We then use this new force interaction model to simulate droplet breakup where the liquid droplets are composed of constituent Lagrangian particles coupled both to each other and the background fluid. Use of molecular dynamics models have been previously shown to reproduce the interfacial behavior of liquid systems, albeit in a different scale regime (e.g., Kulinskii and Maslechko, 2016, Potoff and Panagiotopoulos, 2000; Sinha et al., 2003). We are interested in seeing if the potential models can be adapted to our regime of interest, that of impact dispersal of liquid from fuel tanks.

Here we present some computational methods being developed at Sandia that may be appropriate for the types of problems we are attempting to simulate. Some recent high-fidelity experimental work form the context for assessing the model (Flock et al., 2012). The methods allow for model calibration, and an exercise is described that is used to assess the ability of an under-resolved molecular dynamics liquid model to exhibit drop break-up characteristics in the transitional regime. In this study documentation we term ‘drop’ to be an un-broken incipient liquid, and ‘particles’ as the sub-elements of the original drop.

2. METHODS

2.1 Lennard-Jones methods and theory

Practitioners of molecular dynamics have often modeled liquids (bulk, droplets) using the Lennard-Jones (LJ) potential (Lennard-Jones, 1924). The LJ potential has the following form:

$$U_{LJ}(r) = 4\varepsilon\left[\left(\frac{\sigma}{r}\right)^{12} - \left(\frac{\sigma}{r}\right)^{6}\right] \tag{1}$$

This potential can be thought of as a combination of attractive (~ r^{-6}) and a repulsive terms (~ r^{-12}). The attractive component is physically motivated by London dispersion forces (temporary dipole – induced dipole), whereas the repulsive r^{-12} is an idealized form of repulsive energy likened to the Pauli Exclusion repulsive energy associated with the overlap of electron orbitals. The form itself has no physical basis other than being highly repulsive and mathematically convenient (the square of the attractive term). The Lennard-Jones potential is often employed in atomistic or molecular systems due to its simplicity of form and presence of an attractive well. The two parameters that characterize the LJ potential are the LJ diameter (σ) and energy (ε). The binding energy of two “particles” under LJ is ε, and the minimum of the potential is at a separation of $r_{min} = 2^{1/6}\sigma$. One can readily observe that the number density of a collection of particles

interacting through the LJ potential is $O(1/\sigma^3)$. Likewise, the surface tension γ of a LJ fluid is $O(\varepsilon/\sigma^2)$. Both the density and surface tension are temperature dependent functions which depends on thermal exchange with the background fluid.

While LJ potential model is straightforward to implement, there are disadvantages to using it. One such difficulty comes from the fact that the repulsive component scales as r^{-12} and is quite steep as particles approach each other. The consequence to is that a very small computational timestep is required to resolve the repulsion. Insufficiently small timesteps can result in erratic behavior, the worst of which can be a significant force or kick that a particle receives if it is allowed to approach another particle too closely within the timestep. One could think of this as an artificial thermal energy associated with the pair of interacting particles. Of course, with a small enough timestep, the potential is fully resolved and the interacting pair of particles is stable, though there can always be some small drift in particle positions with time due to the highly nonlinear nature of two interacting spherical particles, as is the case of any central potential. Often one cannot computationally afford the requisite timescale for the steep repulsive part of the LJ potential. One solution to this is the replacement of the repulsive (only) component with a spring potential of the form:

$$U_{spring} = \frac{k}{2}(r - r_{min})^2 - \varepsilon : r < r_{min} \tag{2}$$

This auxiliary repulsive form has a minimum of $-\varepsilon$ at r_{min} just as the LJ potential, that is: $r_{min} = 2^{1/6}\sigma$. The spring constant, k, relates to the Lennard-Jones parameters. Both potentials coincide and have zero slope at this position. The benefit to this form is that a spring potential has a natural oscillation frequency. That is:

$$\omega = \sqrt{\frac{k}{m}} = \frac{2\pi}{T} = \frac{2\pi}{N\Delta t}, \Delta t = \frac{2\pi}{N}\sqrt{\frac{m}{k}} \tag{3}$$

Where ω is the spring angular/oscillation frequency, m is the mass of the particle, N is the number of timesteps of size Δt within one spring period T. Nyquist conditions set $N \geq 2$, however for stability, it is best that N be of order 10 or greater. With this form, we have a definite particle timestep Δt required for stable resolution of the forcefield. The only unknown here is the spring constant k which represents the stiffness of the repulsive term (spring). However, k can be determined if one defines a minimum particle approach point (r_0) and a repulsive energy (U_0) at that approach point. This defines the equation:

$$U_0 = \frac{k}{2}(r_0 - r_{min})^2 - \varepsilon \rightarrow k = \frac{2(U_0 + \varepsilon)}{(r_0 - r_{min})^2} \tag{4}$$

$$\Delta t = \frac{2\pi}{N}(r_{min} - r_0)\sqrt{\frac{m}{2(U_0 + \varepsilon)}} \tag{5}$$

In Figure 1 we display the original LJ potential as well as the modified form of the repulsive component (U_{spring}) with $r_0 = 0.9\sigma$ and $U_0 = U_{spring}(r_0) = U_{LJ}(r_0)$. Notably, the modified repulsive component is not as steep as the LJ potential at r_0, thus allowing for a larger Δt for particle integration. This modified repulsive term has been employed in our current study, with both r_0 and U_0 tunable parameters. Parameters σ and ε are also tunable.

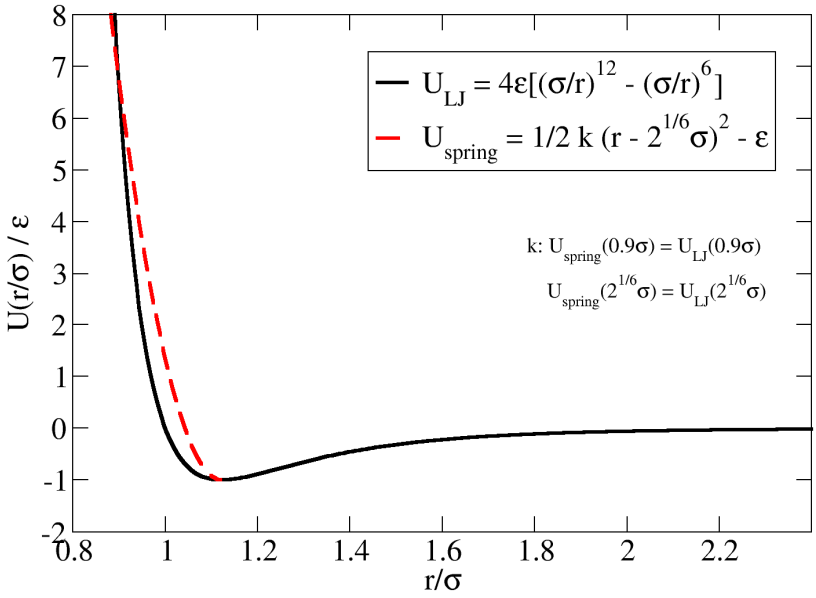

Figure 1: Lennard Jones potential and example of modified repulsive potential. In this case $r_0 = 0.9\sigma$, $U_{LJ} = U_{spring}$ at both r_0 and r_{min}.

One caveat to particle integration in Fuego is that for interacting particles, the Eulerian (fluid) timestep (Δt_{fluid}) can be a limiting factor. While particle timestep subcycling is available, allowing the particles to be integrated at a smaller timescale ($\Delta t_{particle}$) than the fluid, this is currently done one particle at a time (segregated). For N_{sub} particle subcycles, we have $\Delta t_{particle} = \Delta t_{fluid}/N_{sub}$, but assuming that particle A and B will interact, particle A would be integrated and move N times within a single fluid timestep, while particle B would be stationary over this timeframe. Once particle A was completely integrated a full Δt_{fluid}, particle B would then likewise be integrated. This presently requires us to lower Δt_{fluid} to resolve the inter-particle potential within the liquid particle required time step. Work is proceeding to redesign the particle integration routines to allow simultaneous subcycling of all particles in the simulation, but that work is not yet complete.

As previously mentioned, the surface tension γ of a LJ fluid is $O(\varepsilon/\sigma^2)$. Therefore, the model assumes the surface tension is related to the LJ parameters through a single constant:

$$\gamma_{LJ} = C\frac{\varepsilon}{\sigma^2} \tag{6}$$

The constant C can be selected such that the break-up behavior of the particles representing liquid occurs at a physical condition.

2.2 Particle Drag Coefficient Model Modification

In a bulk particle model, a particle that is internal to a drop should not experience interactions with the gas phase velocity. The interaction should come via a coupling through surface particles. Also, lee-side surface elements should not experience the same magnitude of drag as do wind side particles. We expect the liquid/gas interaction forces in that case to be smaller. The cases we have been running exhibit far too much responsiveness to the wind flow, as the cumulative drag is too high when modeling the particle effect individually (drag goes as surface or wetted area, which is artificially too high by a significant amount, increasingly so for increasing levels of refinement).

We desire a simple way to better model the above desired behavior that doesn't require expensive surface reconstruction or iterative searches. A model form is proposed that simply modifies the drag coefficient

term C_{Do} for a particle independent of any connectivity. The modified drag coefficient, C_{Dm}, is a function of the independent drag term and a scaling factor, f_S:

$$C_{Dm} = f_S C_{Do} \tag{7}$$

Target features of the scaling factor need to be that it is unity when a particle is minimally influenced by a neighboring element with respect to the wind. When a particle is clustered internally (not exposed to air, or not on the surface), it should approach zero. When a particle is a surface element on the wind side of a larger drop, it should be near unity. On the lee side surface of a particle, the drag term should go to zero. The model needs to be applicable for a variety of coordination numbers (N) that reflect a count of the number of particles between which interaction forces are being applied.

Consider breaking the scaling factor, f_S, into two components. One component tests whether the particle is internal (surrounded by others) or not. If internal, the factor goes to zero. If not, it remains unity. The other component tests whether the windward condition exists, and stays unity if the particle is windward, goes to zero if it is lee-side. The scaling factor, f_S, is then composed of two components:

$$f_S = f_{S1} f_{S2} \tag{8}$$

Component f_{SI} will test the internal/external particle condition. This is done first computationally for reasons that will be clear later. To have a model behave correctly, we want the model to identify if there is a dominant direction to the connecting particles. This can be determined by looking at the mean vector direction of all connections. If connections surround one side of the particle, there will be a dominant direction and a sizeable magnitude of a vector in that direction. If the particle is surrounded, the vector magnitude will be small. The model question then becomes how to sum and scale the existing vector field of particles interacting with the source particle such that we achieve the unity condition for surface particles and the zero condition for internal particles. We may get a good answer if we impose arithmetic addition of the position vector components. This method will skew against close particles, and favor distant particles, which might be a problem if the particles are not well spaced or if we artificially limit the coordination number to skew the answer. It is not clear if either of these problems will exist in real conditions (we will want to look for this in an initial implementation). The equation for the first (proposed) scaling factor component can then be easily calculated from existing model information:

$$f_{S1} = max\left(1, \frac{\left[\left(\frac{\sum_{i=1\to N}(x_o - x_i)}{N}\right)^2 + \left(\frac{\sum_{i=1\to N}(y_o - y_i)}{N}\right)^2 + \left(\frac{\sum_{i=1\to N}(z_o - z_i)}{N}\right)^2\right]^{1/2} N}{\sigma}\right)^K \tag{9}$$

Here, σ is the Lennard-Jones length-scale parameter (which should be approximately the distance between the source and connected particles), N the coordination number, x, y, and z are the Cartesian coordinates of the particles, and the subscripts o are for source particles and i for the N affecting particles. If the source particle is surrounded, then the number inside the brackets should be small, and the scaling parameter will be small (much less than unity). If one direction is dominant, then the number in the bracket will be comparatively large. The scaling parameter will be comparatively large, perhaps unity. There is a small likelihood of the scaling parameter being zero, in which case an undefined condition will exist in the computation of the second scaling parameter. If the first scaling parameter is zero, then the next step needn't be taken (the answer is trivial anyhow, and the zero condition in the first parameter upsets the calculation of the second parameter).

Component f_{S2} will test the windward/lee-side condition. Here we want a function that compares the direction of the wind velocity with the direction of the particle free face. If they are in opposite directions, we want the scaling parameter to be unity. As they align, we want the value to go to zero. Take the velocity unit vector (u-hat) relative to the velocity frame of the drop/particle:

$$\hat{u} = \frac{\vec{u}}{|u|} \tag{10}$$

Then compose a unit vector that is the mean connectivity vector (note that two equations above we are taking the magnitude of this same mean connectivity vector, which allows for a simplified description of that formula):

$$\vec{k} = \left\{ \frac{\sum_{i=1\to N}(x_o - x_i)}{N}, \frac{\sum_{i=1\to N}(y_o - y_i)}{N}, \frac{\sum_{i=1\to N}(z_o - z_i)}{N} \right\} \tag{11}$$

$$\hat{k} = \frac{\vec{k}}{|k|} \tag{12}$$

With this definition for the connectivity vector, the above formula for f_{S1} can be simplified to:

$$f_{S1} = max\left(1, \left(\frac{|k|N}{\sigma}\right)^K\right) \tag{13}$$

k-hat points towards the inside of the particle (the outward condition is the negative of k-hat). The projection of u-hat onto k-hat is simply the dot product of the vectors:

$$Proj = \hat{u} \cdot \hat{k} \tag{14}$$

If the vectors are in the same direction, the projection will be positive. If they are opposing, it will be negative. Since we are dealing with unit vectors, the product is constrained to $-1<Proj<1$. The model for the second scaling factor is then:

$$f_{S2} = min(1, 1 + Proj)^L \tag{15}$$

2.3. Simulation Scenarios

To test the new formulation, it is desirable to have a validation dataset or physical reality to guide the work. Aerodynamic drop break-up has been studied in the past, and the work of Guildenbecher and co-workers (Flock et al., 2012) has recently been yielding comparatively high fidelity experimental measurements of drop break-up in a flow. Historically, this area of research was characterized by Faeth and co-workers Hsiang and Faeth, 1992), who identified a critical Weber number characterizing the on-set of break-up for liquid drops. The critical Weber number for break-up was found to be about 12, below which there was no break-up and above which break-up occurs. The Weber number is defined differently for various studies. Here, the Weber number is defined as:

$$We = \frac{\rho_a u_0^2 d}{\gamma} \tag{16}$$

The density is the *air* density, and the velocity is the differential between the free-stream air flow velocity and the drop. Guildenbecher and co-workers produced images illustrating the break-up and transitional behavior.

The constant C in Equation 6 relating the Lennard-Jones parameters to the surface tension requires calibration. Having implemented the theory described above, an exercise was required to select the constant that will reproduce the transitional break-up that occurs at about *We=12*. The transition is thought to be a good target for calibration because of the significant difference in outcome achieved above and below the transition point in the tests.

The experiment involved a circular air nozzle with an exit diameter of 25.4 mm and an ethanol drop of 2.52 mm diameter released 9 mm downwind of the exit plane of the nozzle and 174 mm above the centerline. An appropriate domain for modeling this scenario was constructed using a fairly coarse mesh. This assured that the drop was not a major component of any computational cells, which would violate the dilute spray requirements for the model were it true. At time zero, the drop was started at the initial location and allowed to drop via gravity towards the air jet, which was also started in the model at time zero. A laminar flow assumption was employed for the CFD, which means that turbulent characteristics of the jet were not modeled.

The model employed particles of varying sizes, which was desirable to demonstrate any dependency of the model on resolution. The lowest resolution scenario involved a single particle and used the TAB model for break-up. The next highest resolution involved 19 particles, up to 767 particles for the finest case. Because the particle solves were segregated, there was a severe (small) time step requirement to maintain stability. All scenarios were run with a global time step of 10 μs, which in an earlier phase of modeling was shown to result in consistently stable results. Initial particle clouds composing the drop were created with a script algorithm that created a face centered cubic (FCC) block in which a best fit sphere of particles was retained. Thus, the particles were all in equal proximity and stable at the time of initiation. A particle characteristic length was selected, and on that basis the FCC pseudo-spherical block was generated together with the corresponding number of particles. The volume of the particles using the nominal diameter did not match the volume of the drop (due to void spaces in the FCC matrix), so the particle radius was adjusted to conserve mass and volume. This resulted in all drops having an identical volume, and also resulted in some overlap between particles at a stable condition. The Lennard-Jones separation distance parameter did not match the nominal diameter either due to geometric considerations relating to the FCC matrix. The Lennard-Jones sigma parameter was the nominal particle diameter divided by $2^{1/6}$. Table 1 lists the various drop model assumptions. The well depth (energy, or ε) term for the L-J model was calculated using Equation 6, and the surface tension was assumed to be 0.0221 N/m corresponding to ethanol in an atmosphere of air at room temperature. Preliminary testing with coarser simulations runs suggested a constant C of about 200 gave break-up results in the correct regime. All results shown here are with that constant.

Table 1. Drop model assumptions

Scenario	# particles	Particle Nominal Diameter *mm*	L-J Diameter (σ) *mm*	Volume Corrected Diameter *mm*	L-J Well (ε) *J*
TAB	1	2.52	NA	NA	NA
R1	19	0.75	0.668	0.944	4.93e-11
R2	87	0.50	0.445	0.568	2.19e-11
R3	177	0.40	0.356	0.449	1.40e-11
R4	321	0.33	0.294	0.368	9.55e-12
R5	767	0.25	0.223	0.275	5.48e-12

The drag limiter model was on with N (the coordination number) resulting from a neighbor search terminating 1.5-sigma away from a source particle. The constants K and L are assumed to be 1.0 for now, but will be calibrated in subsequent work.

Five jet velocity conditions were tested. The velocity conditions and corresponding Weber numbers are found in Table 2. The 9 m/s velocity condition was believed to be at the transition point, or critical Weber number. Drops with higher Weber numbers should shatter, whereas lower Weber number drops should not.

Table 2. Nozzle flow conditions and corresponding Weber number and expected outcome

Nozzle Velocity *m/s*	Weber Number -	Expected Outcome
3	1.23	No Break-up
6	4.93	No Break-up
9	11.08	Transitional
12	19.70	Break-up
20	54.73	Break-up

3. RESULTS AND DISCUSSION

The drag correction terms are still a work in progress. This is apparent in the results, as the scenarios with increasing particle counts exhibit increasing drag and consequently arrive at the nozzle at a later time. Ideally, all drops would fall at the same rate and would arrive at the nozzle simultaneously. The present model does not exhibit full drag corrective capability, but represents an improvement on the use of no drag limiter. The work is presented here because it enables the illustration of the break-up modeling, which is at a more mature state and is the main topic of this paper.

3.1 Drop break-up with the L-J model

The break-up behavior is illustrated visually by superimposing the results of the different simulations on the same image. The problem with direct superposition is that this results in significant overlap between the falling drops. For clarity, they are separated by progressively transforming drops 0.3 cm in the downstream direction (ordered with increase in jet flow velocity).

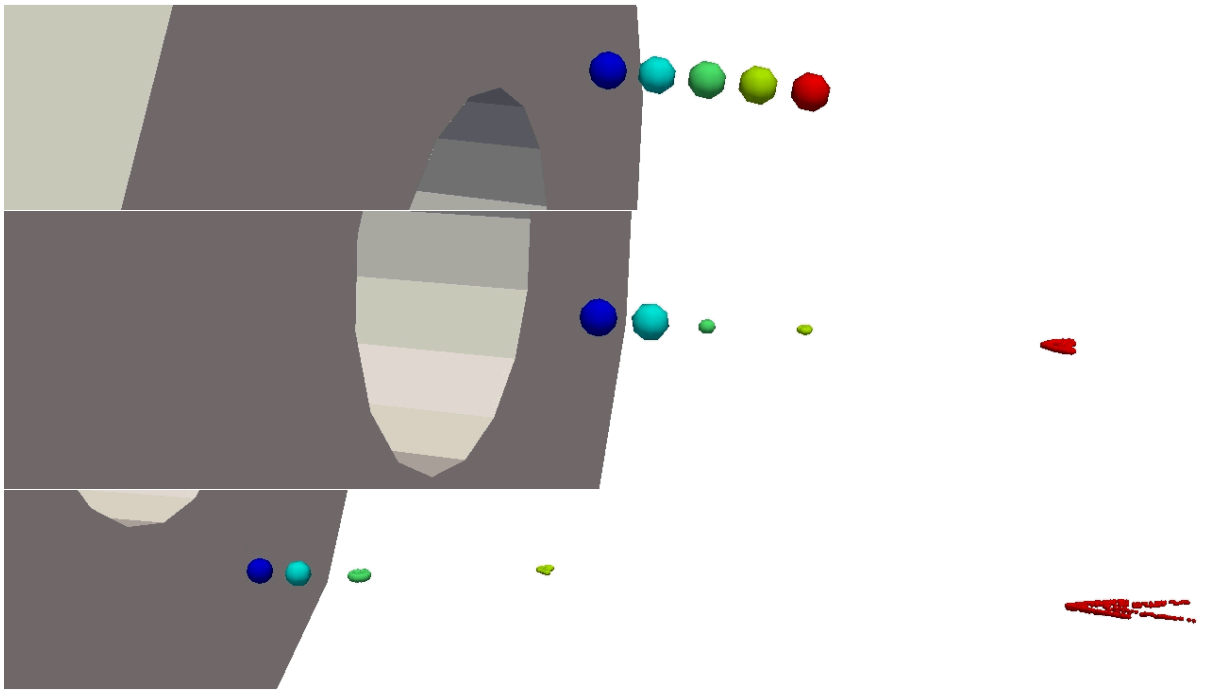

Figure 2. TAB scenario results before (top), during (middle), and after (bottom) passing through the jet

Break-up is judged in this case to be when the particles separate significantly after passing through the air jet from the nozzle. A visualization of the drops before, during, and after passing through the flow are reproduced in Figures 2-7 for the six scenarios listed in Table 1. Particles are colored by the *jet* velocity, and are also arranged such that from left to right the velocities are 3, 5, 9, 12, and 20 m/s (blue to red). The circular nozzle is illustrated to the left of the drops, and air flows from left to right. Figure 2 shows TAB model results. The 3 and 6 m/s drops do not shatter, whereas the higher velocities induce break-up. Because the TAB model simply creates daughter particles at the center of the mother particle, there may particle overlap and this may be incorrectly interpreted that the results are not volume or mass conservative. This is not the case. Particle mass is allowed to occupy the same volume, and the particles only separate with time as they move apart due to advective processes.

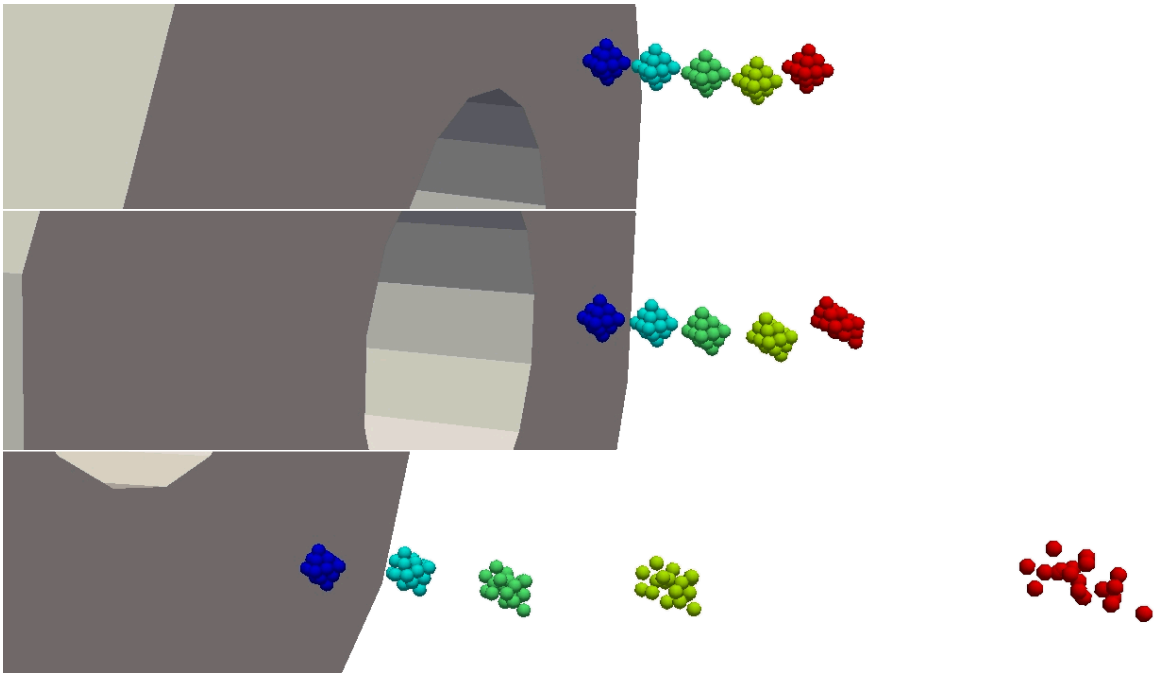

Figure 3. R1 scenario results before (top), during (middle), and after (bottom) passing through the jet

Figure 3 shows scenario R1 results. The drops for 12 and 20 m/s clearly break-up, whereas the others are not as obviously broken up. The 9 m/s scenario exhibits some particle separation, but it is not obvious whether the drop is just perturbed or if it is fully broken. At later times (not pictured), the break-up becomes more obvious. The 6 m/s scenario appears to result in a deformed drop after passing through the flow field, but is not apparently broken. The drop that passed through the 3 m/s jet exhibits no indication of break-up. It does appear to rotate slightly.

Figure 4 shows results from the R2 scenario. The drops that passed through the 9, 12, and 20 m/s jets are clearly broken up, and the 6 m/s scenario exhibits some potential break-up at the perimeter. Internal break-up is not obvious.

Figure 5 shows results from the R3 scenario. It exhibits similar behavior as did the R2 scenario.

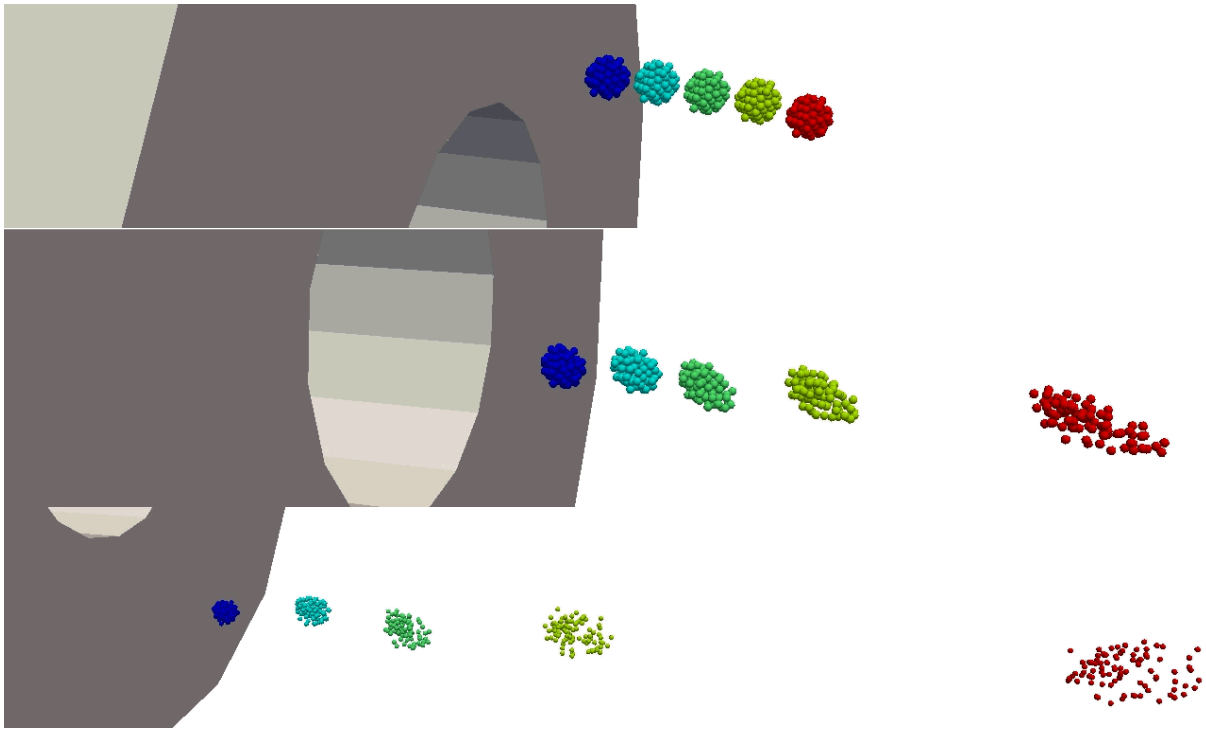

Figure 4. R2 scenario results before (top), during (middle), and after (bottom) passing through the jet

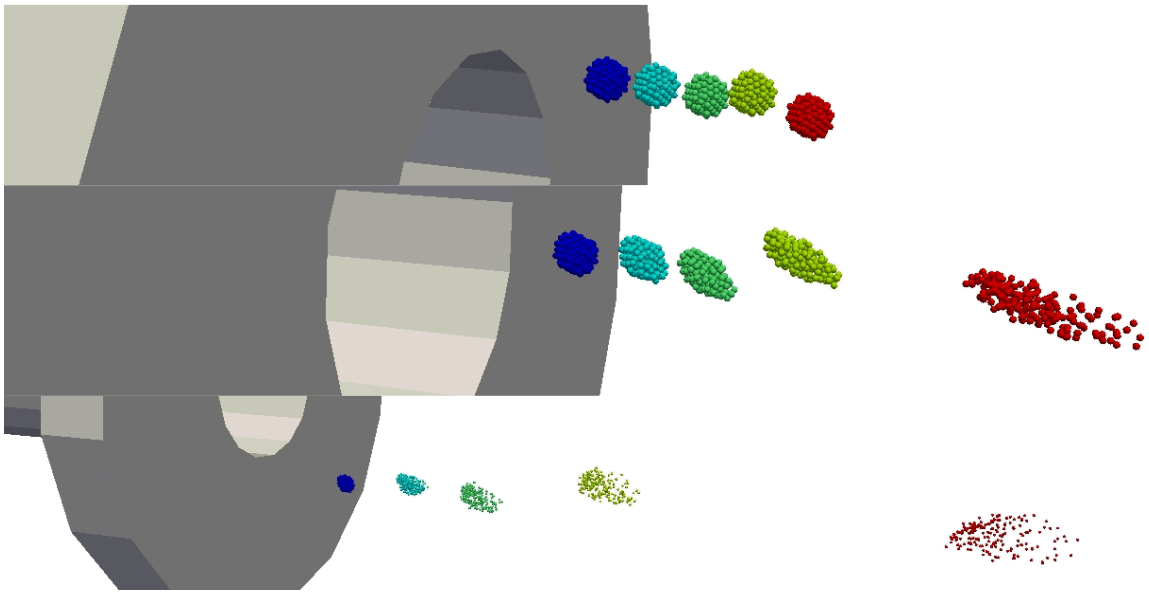

Figure 5. R3 scenario results before (top), during (middle), and after (bottom) passing through the jet

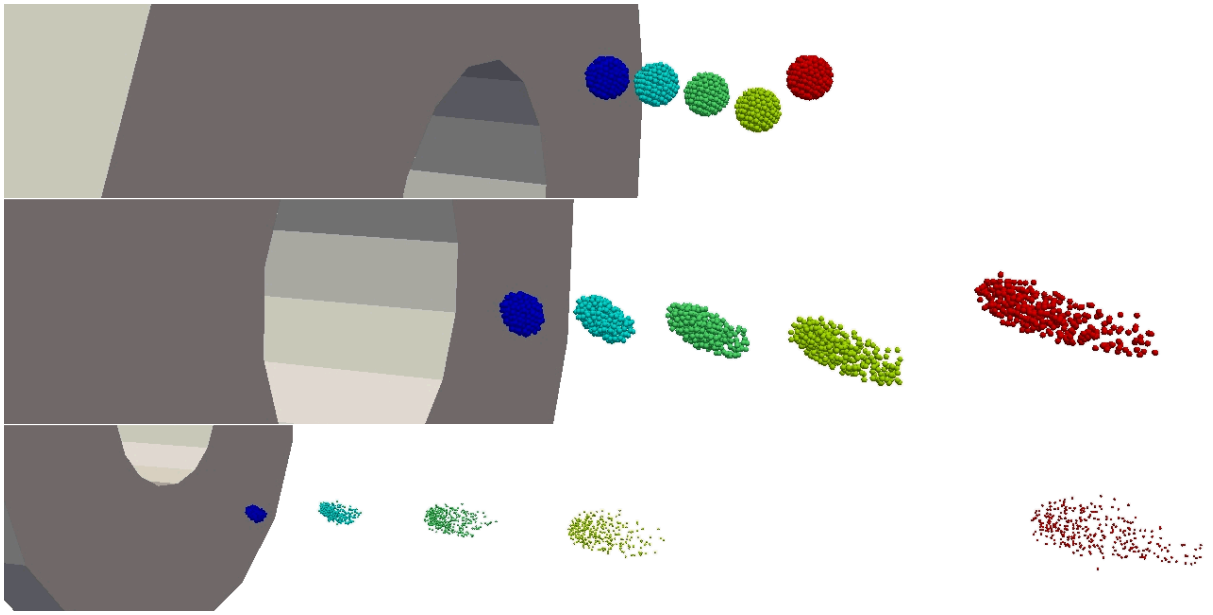

Figure 6. R4 scenario results before (top), during (middle), and after (bottom) passing through the jet

Figure 6 shows results from the R4 scenario. One main difference in this scenario and scenario R3 and R2 results noted here is that the drop subjected to a 6 m/s jet shows a clearer indication of break-up. The drop subjected to the 3 m/s jet appears to be somewhat distorted.

Figure 7 shows results from the R5 scenario. As with the R4 scenario, the 6 m/s scenario exhibits break-up, and the 3 m/s scenario drop exhibits significant distortion.

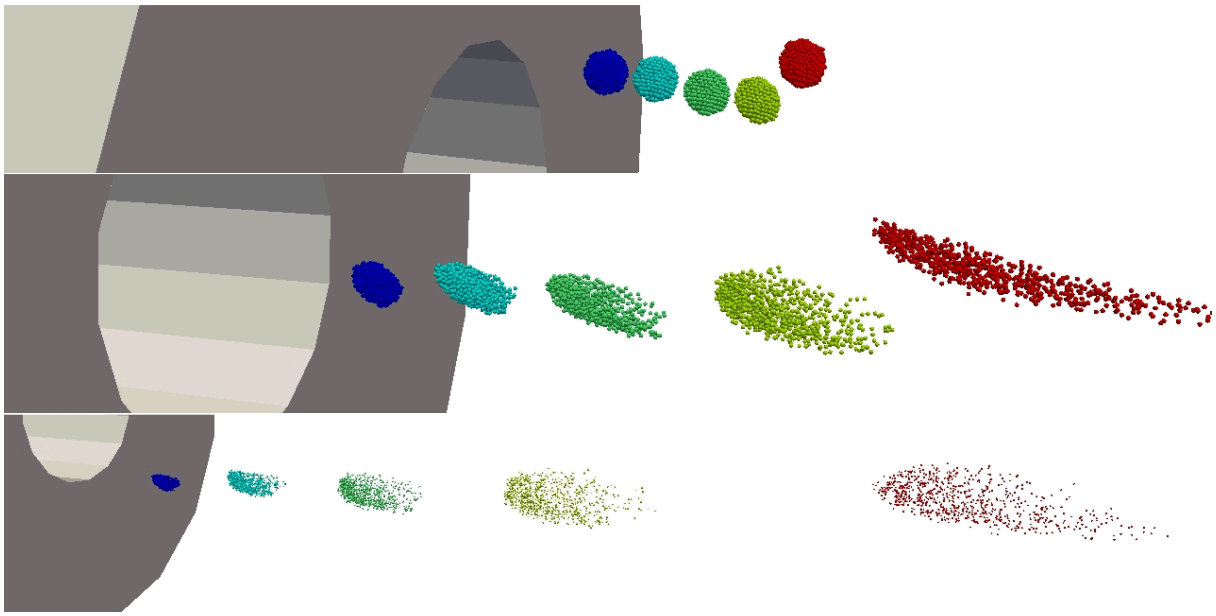

Figure 7. R5 scenario results before (top), during (middle), and after (bottom) passing through the jet

With the constant *C* selected to be 200, the break-up behavior of the L-J model is approximately correct. The 6 m/s case should not break up, but exhibits onset or full break-up in most of the cases (excepting, perhaps, R1). This suggests that the initial constant selection of 200, although good, may be slightly high.

Reducing it has the effect of an increasing inter-particle force, and will help the 6 m/s scenario drops stay together as historical testing suggests they should. Visual observations of the drops suggest the 3 m/s scenario does not result in break-up, however there are indications of onset in the more refined cases. This too should be remediated by a decrease in the model constant.

The TAB model exhibits break-up for the 9 m/s and above cases. Although it may not be obvious in the results plots, the higher jet speed results in smaller drops. The other scenarios, R1 through R5 seem to yield mostly clouds of secondary drops sized according to the particle diameters as listed in Table 1. It might be expected to see groups of particles for the scenarios with the most particles that could be interpreted as the largest particles in a distribution of product particles. This was not clearly observed in any results. The R1 scenario, conversely, might be thought to yield particles that are too big simply because of the defined particle size. The TAB model results suggest the R1 scenario particles may be too large. If the model were to allow for physical break-up to first occur due to particle separations using the L-J analogy methods, it might then be appropriate to activate the TAB model on separated particles to achieve further break-up. This does not appear to be the break-up mechanism in the experimental studies, but such an approximation may give a more accurate result.

The break-up mechanism in the literature at about *We=12* is bag break-up or bag and stem (see Flock et al., 2012). This involves the flattening of the drop when it passes into the flow, followed by the "inflating of the bag" resulting in a very thin hemispherical film. This film ruptures, which seems to result in the satellite particles. This behavior is not exhibited in any of these results. The reason for this could be due to limitations to the drag model. It might also relate to the mesh resolution. The fluid mesh was fairly coarse in these calculations, and likely produces a velocity gradient much different than that from the tests. This can be improved in future work. A third reason the bag shape did not form might be due to close small-scale dynamic interactions between the liquid and gas. This approach cannot be expected to resolve that behavior as the method by design requires that the drops be smaller than the fluid mesh.

It may be noted in the top frames of Figures 3 through 7 that the initial drop height varies. In Case R1, R4, and R5, the drop falling into the 20 m/s jet appears to lag the others. The same lag is not present for Case R2 and R3, which suggests that the issue is not related to the jet velocity alone. This variation is thought to be related to the drag model via instantaneous and small variations in the drop internal spacing as it falls. It is not believed to be representative of some other systematic problem with the input files, as that has been verified by comparing input files for the simulations. The fact that the 20 m/s scenarios exhibited some similarity in their variation from the mean is thought to be coincidental.

3.2 Drag Limiter Model

The f_{S1} model resulted in external particles with an f_{S1} value of about 1.0, with internal particles near zero at first, but closer to 0.5 for a moving and oscillating drop. This is thought to be due to minor internal movement induced by particle drag that naturally occurs in an oscillating system such as this. Increasing the factor K can help this model to achieve f_{S1} values of near zero for internal particles and 1.0 for external particles, which is the desired behavior. The f_{S2} model typically resulted in values between 0.9 to 1.0, and consequently is thought to have had a minor effect on the outcome. Kinetic energy is used as a comparison metric between the scenarios. As all scenarios have the same mass (we did not allow evaporation), kinetic energy is also a scaled expression for integrated velocity. Figure 8 shows a plot of the drop kinetic energy versus time for each prediction. These scenarios would ideally yield the same results. Notice first the differences in the 0.05 to 0.15 second range. These differences are due to the drag model methods employing particle drag to compute drop drag as an assembly of that predicted for the composition particles. The TAB prediction can be taken as the ideal result. Thus, the higher refinement scenarios are increasingly affected negatively by the drag assumptions in the model. The R5 case does not appear to achieve half the kinetic energy of the TAB model results, which suggests a need for a significant improvement in the drag model for scenarios with high levels of liquid refinement. The R1 scenario exhibits small differences, which suggests that the model may be approximate for the coarser scenarios. Notice in the 0.19 to 0.22 second time range that there is an inflection. This corresponds to the particle first interacting with the jet. The inflection is small for the TAB, and the R1 scenarios. It is increasingly large for the R2 up to R5 scenarios. In the case

of TAB and R1, the inflection is small because the break-up of the drops results in larger particles than the R2 through R5 scenarios. Larger particles exhibit less drag, and consequently do not exhibit as much of an increase in kinetic energy. The TAB model should not be treated as truth in this case, as it exhibits only an approximate behavior for break-up. It would be a productive effort to quantify drop kinetic energy in future efforts so a measure of liquid kinetic energy could be used for model validation. There is a subsequent inflection in most cases, which corresponds to the drop leaving the air jet. The drop-off in kinetic energy to zero at the end of each line trace represents the particles leaving the computational domain, the transition to which corresponds to the last inflection in each case.

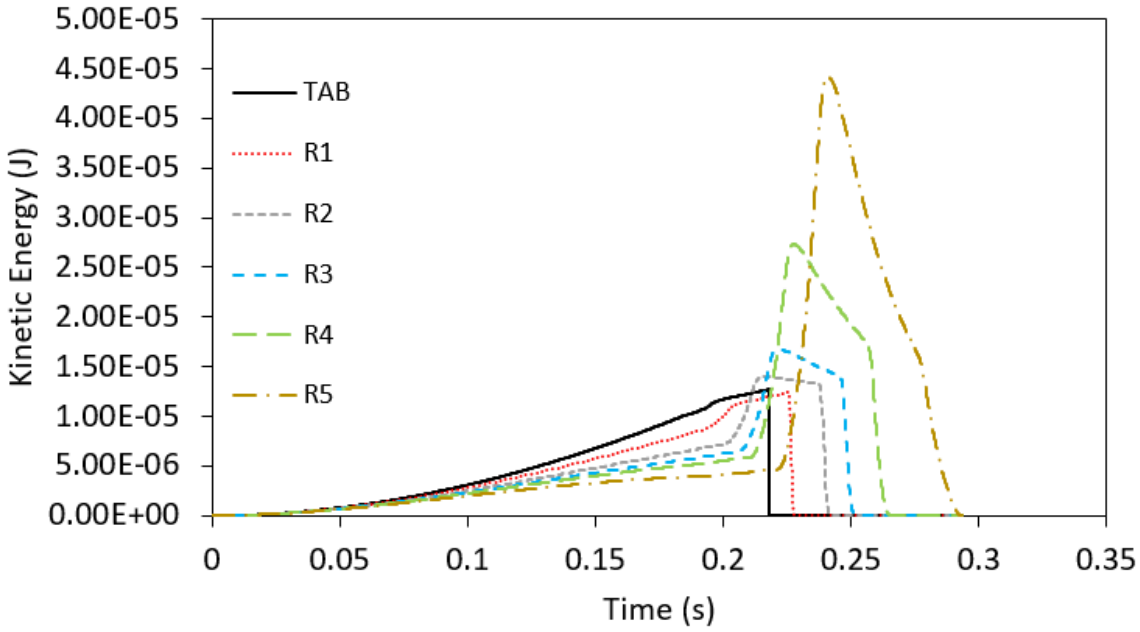

Figure 8. Drop kinetic energy for the 9 m/s jet scenarios

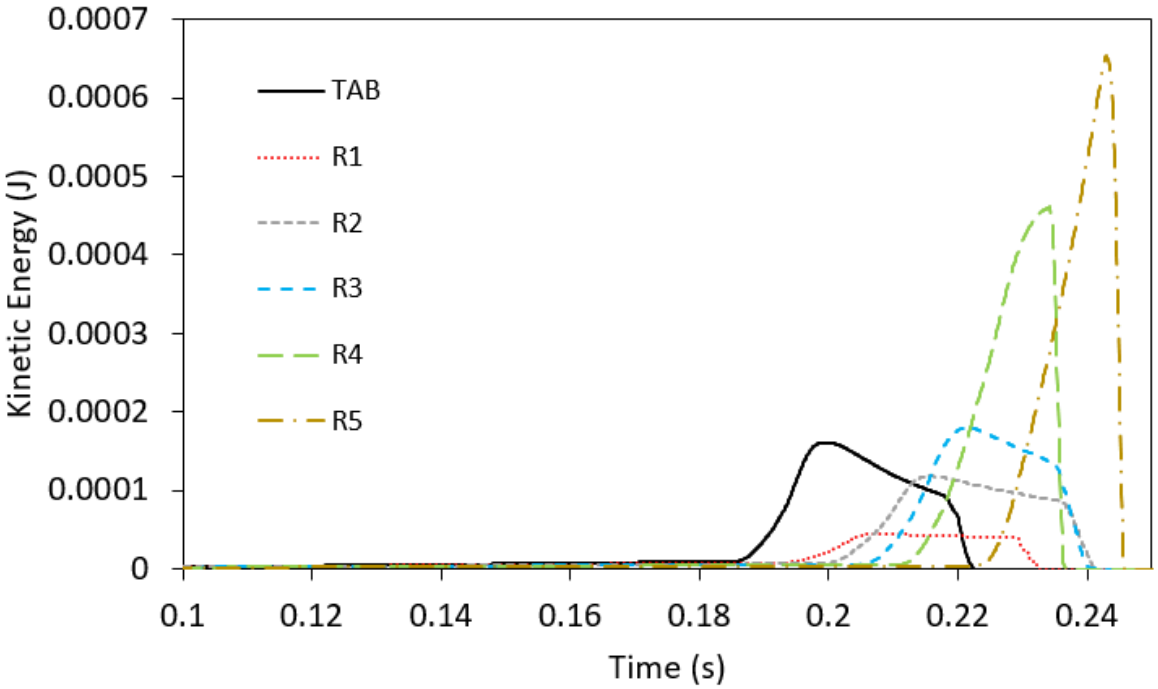

Figure 9. Drop kinetic energy for the 20 m/s jet scenarios

Figure 9 shows a similar plot for the 20 m/s jet scenarios. Because there is significantly more kinetic energy, the falling particle kinetic energy (times < 0.18 seconds) is low and not as resolved at the scale of the plot. It looks like Figure 7 results, so this plot was adjusted for the scale to show the peak values of kinetic energy. Unlike the 9 m/s scenario, the TAB model more closely resembles in peak magnitude the R2 and R3 scenarios instead of the R1 scenario. This is because the TAB model predicts particle sizes closer to that of those two scenarios.

Evaluating the kinetic energy of the various predictions demonstrates a significant spread in prediction results of the L-J model depending on the initial resolution of the drops. One component of the problem relates to the over-prediction of aerodynamic drag on the particles. This model is a work in progress, and will be improved in subsequent work. The other component of the problem relates to the particle size dependency (resolution dependency) on the break-up dynamics. This issue will require attention as well in subsequent work.

4. GENERAL DISCUSSION

A very strong positive to these results is that the drop break-up for various levels of refinement appears to be representable by the surface tension and a single scaling constant through the L-J parameters. Comparing R1 to R5 results, the onset of break-up of the drop was fairly consistent, despite the factor of 3 difference in particle diameter and 1-2 orders of magnitude difference in the number of particles. We are thus optimistic that this model may constitute a good method for simulating bulk liquid behavior in complex scenarios where structural dynamics and fluid dynamics codes are coupled to solve impulse or impact dispersal of liquids. It remains to be seen how the fit constant parameter scales with larger particles, as this experimental test case did not accommodate particles larger than the original drop.

Some of the results do not look particularly promising in the figures presented above, particularly at the highest levels of refinement (R4, R5). It is important to keep in mind the application space driving this implementation. The incipient particles in historical work (see Brown and Pierce, 2015) are typically much

larger than was the case for this validation scenario. The drop size was only 2.5 mm diameter in this work, and some of the previously described scenarios (see Brown et al., 2015) had particles of an order of magnitude greater in size. Thus, the R1 scenario is thought to be the most representative behavior of the model in the regime of interest, although application space can be significantly coarser. The drag correction error is more subtle for larger particles and larger particle clusters. The very refined drop simulations were not intended to be the ideal convergent answer for the drag and break-up models, although it would be nice if they were demonstrated to be convergent. The scenario that was selected for evaluating model behavior is in a good and well characterized experimental regime, but is not particularly close to the regime of interest for the historical use of the model. It will be helpful in the future to evaluate the behavior for larger scale systems. The R1 results are the closest to the regime of interest, and those results were generally promising.

As has been alluded to previously, the current break-up model cannot directly model break-up of particles beyond the point where the L-J forces become negligible. This is because TAB is not presently active for particles that are connected with the L-J model. This fact should not preclude the formation of smaller drops in more complex flow conditions. Experimental results seem to suggest the coarse L-J and TAB models may under-predict the break-up for drops near the inception point. Very small particles can emerge from bag break-up (see Flock et al., 2012). We anticipate incorporating the TAB model in conjunction with the L-J model to allow further break-up. This would likely result in the 20 m/s jet R1 scenario exhibiting further break-up, and potentially exhibiting a kinetic energy profile more similar to that of the TAB scenario and other L-J scenarios as illustrated in Figure 9. This is not expected to result in the R1 scenario exhibiting further break-up in the 9 m/s scenario. Additional work may need to be done for the drop break-up near the inception regime. An advantage of the current method is the ability to spatially distribute the mass better than the TAB model, which can result in particles that are overlapping in space.

While good data exist for small drops in high air flow jets, the data are scarce for large drops in low flow jets. This type of data may be more relevant to this application space, and would be an interesting addition to the body of work on aerodynamic drop break-up.

The drag correction model needs additional attention. The exponent parameters K and L were selected to be 1.0 in all of this work. These will be modified with the intent of improving the drop behavior making it more consistent for drops composed of different particle counts. There is an additional constant, which is a search distance parameter for determining coordination number. These parameters need fitting, which will occur in future work. It is not clear at this point that the drag correction model will be able to achieve independence of scale, in which case there may be need to resort to a potentially more costly method like the ones described above relating to the PFEM model (Idelsohn et al., 2004). There is also need to see if the L-J surface tension model constant, C, is universal. This would require additional testing with different fluids and particle scales.

5. CONCLUSIONS

A model has been proposed for simulating liquid-like particle interaction in a dilute spray CFD code using molecular dynamics analogy methods with the aim of reproducing drop break-up behavior. The constitutive parameters are modeled via a single fit constant (not including the Lennard-Jones parameters, which are considered physical parameters), which appears to exhibit reasonably good universality over the range of drop refinement tested. This is demonstrated in the ability to predict drop break-up close to the critical Weber number determined from historical experimental characterization for a range of particle size resolutions. The current proposed drag limiter model needs additional work, but exhibits a behavior that may lead to a reasonably predictive capability after appropriate adjustments are made.

ACKNOWLEDGMENT

Dan Guildenbecher kindly provided a review of the initial simulation results, which resulted in an improved representation of the experiments in the simulation exercise. Manuscript reviews by Dan Guildenbecher and

Heeseok Koo are also appreciated. Sandia is a multiprogram laboratory operated by Sandia Corporation, a Lockheed Martin Company, for the United States Department of Energy under Contract No. DE-AC04-94AL85000.

REFERENCES

[1] Brown, A.L., G.J. Wagner, and K.E. Metzinger, "Impact, Fire and Fluid Spread Code Coupling for Complex Transportation Accident Environment Simulation," Journal of Thermal Science and Engineering Applications, Vol. 4, No. 2, pp. 021004-1 to 021004-10, June (2012).

[2] Brown, A.L., and Pierce, F., "A Modeling Method for Impact and Impulse Dispersed Liquids: Alternative Transfer Criteria and Sensitivity Analysis," ILASS Americas, the 27th Annual Conference on Liquid Atomization and Spray Systems, Raleigh, NC, May (2015).

[3] O'Rourke, P. J., and Amsden, A.A., "The TAB Method for Numerical Calculation of Spray Droplet Break-up," SAE Technical Paper 870289, (1987).

[4] Brown, A.L., Metzinger, K.E., and Wagner, G.J., "Methods and Findings from Combined Environment Transportation Impact and Fire Predictions Employing Coupled Structural Dynamics and Computational Fluid Dynamics," the 11th International Symposium on Fire Safety Science, Christchurch, NZ, February 10-14, 2014.

[5] Idelsohn, S.R., Oñate, E., and Del Pin, F., "The particle finite element method: a powerful tool to solve incompressible flows with free-surfaces and breaking waves," Int. J. Numer. Meth. Engng., 61, pp. 964-898, (2004).

[6] Herrmann, M., "A sub-grid surface dynamics model for sub-filter surface tension induced interface dynamics," Computers & Fluids, 87, 92-101, (2013).

[7] Rana, S., and Herrmann, M., "Primary atomization of a liquid jet in crossflow," Physics of Fluids, 23:9, (2011).

[8] Herrmann, M., Arienti, M., Soteriou, M., "The impact of density ratio non the liquid core dynamics of a turbulent liquid jet injected into a crossflow," Journal of Engineering for gas turbines and power-transactions of the ASME, 133:6, (2011).

[9] Bertolotti, F.P., Th. Herbert, and P.R. Spalart, "Linear and nonlinear stability of the Blasius boundary layer," J. Fluid Mech., 242, 441-474, (1992).

[10] Cheung, L.C., and T.A. Zaki, "A nonlinear PSE method for two-fluid shear flows with complex interfacial topology," Journal of Computational Physics, 230, 6756-6777, (2011).

[11] Fox, R.O., F. Laurent, and M. Massot, "Numerical simulation of spray coalescence in an Eulerian framework: Direct quadrature method of moments and multi-fluid method," Journal of Computational Physics, 227, 3058-3088, (2008).

[12] Hsiang, L.-P. & Faeth, G. M. "On the breakup of accelerating liquid drops," Intl J. Multiphase Flow 18, 635–652 (1992).

[13] Theofanous, T.G., Li, G.J., Dinh, T.N., and Chang, C.-H., "Aerobreakup in disturbed subsonic and supersonic flow fields," J. Fluid Mech., 593, pp. 131-170, (2007).

[14] Flock, A.K., Guildenbecher, D.R., Chen, J., Sojka, P.E., and Bauer, H.-J., "Experimental statistics of droplet trajectory and air flow during aerodynamic fragmentation of liquid drops," Int. J. Multiphase Flow, 47, pp. 37-49, (2012).

[15] Sierra Thermal Fluids Development Team, "Sierra Fuego Theory Manual – Version 4.40," Sandia National Laboratories, SAND 2016-4155, (2016).

[16] Sierra Thermal Fluids Development Team, "Sierra Fuego User Manual – Version 4.40," Sandia National Laboratories, SAND 2016-4157, (2016).

[17] Kulinskii, V.L., and A. Maslechko, "Surface Tension of the Liquid-Vapor Interface of the Lennard-Jones Fluids from the Ising Model," Journal of Physical Chemistry C, 120, 8790-8803, (2016).

[18] Potoff, J.J., and Panagiotopoulos, A.Z., "Surface Tension of the 3-Dimensional Lennard-Jones fluid from Histogram-Reweighting Monte Carlo Simulations," J. Chem. Phys, 112, 6411-6419, (2000).

[19] Sinha, S., Dhir, V.K., Shi, B., Freund, J.B., and Darve, E., "Surface tension evaluation in Lennard-Jones fluid system with untruncated potentials," Proceedings of the 2003 ASME summer heat transfer conference, HT2003-47164, (2003).
[20] Lennard-Jones, J.E., "On the Determination of Molecular Fields," Proc. R. Soc. Lond. A, 106, 738, 463-477, (1924).